Spin-exchange kinetics of excitons in Cu_2O: Transverse acoustic phonon mechanism

J. I. Jang, K. E. O'Hara, and J. P. Wolfe
Physics Department and Materials Research Laboratory, University of Illinois at Urbana-Champaign, 1110 West Green Street, Urbana, Illinois 61801, USA

(Received 29 January 2004; published 10 November 2004)

The interconversion between orthoexcitons and lower-lying paraexcitons in Cu_2O is studied by time resolving the orthoexciton and paraexciton luminescence following picosecond photoexcitation. The buildup of paraexciton numbers and the orthoexciton decay are observed over the temperature range 2–20 K. The low-temperature limit of the conversion rate is accurately measured. The temperature dependence of the interconversion rate suggests that the dominant mechanism for ortho-para interconversion is the emission or absorption of a single transverse acoustic (TA) phonon. We propose a microscopic model in which rotation of the lattice induces the spin flip through spin-orbit coupling. The energy splitting between orthoexcitons and paraexcitons is modified by applying stress to the crystal, and the the interconversion rate as a function of this splitting is found to be consistent with the single TA phonon mechanism.

DOI: 10.1103/PhysRevB.70.195205 PACS number(s): 71.35.Cc, 72.10.Di, 72.15.Lh

I. INTRODUCTION

Cu_2O is a direct-gap semiconductor with a band gap of 2.173 eV.[1] The exciton, or bound electron-hole pair, in this crystal consists of a hole in the highest valence band ($^2\Gamma_7^+$) and an electron in the lowest conduction band ($^2\Gamma_6^+$). Both these bands possess even parity, resulting in long exciton lifetimes. The excitonic binding energy is 150 meV, and the ground state is split by the exchange interaction into a triplet-state *orthoexciton* ($^3\Gamma_{25}^+$) and a singlet-state *paraexciton* ($^1\Gamma_2^+$), with a splitting energy of $\Delta = 12$ meV. The mechanism for interconversion of orthoexcitons and paraexcitons has been the subject of interest since the early 70's.

Renewed interest in the kinetics of orthoexcitons and paraexcitons came with numerous attempts to observe Bose-Einstein condensation of excitons in this crystal.[2] The difficulty in reaching the condensed state lies in a strong two-body recombination rate at high densities.[3] It is generally believed that the kinetics and thermal equilibration of excitons depend on two key processes: ortho-para conversion[4–6] and Auger recombination.[7,8]

In this paper we take a fresh look at the ortho-para conversion process. For the first time both paraexciton and orthoexciton populations are monitored, taking care to calibrate the relative densities. We present both temperature and stress dependence of the interconversion rate. We present a microscopic model involving the emissions of a single transverse acoustic (TA) phonon.

The first studies involving ortho-para conversion in Cu_2O were reported by Kreingold and Marakov,[4] who measured [with continuous wave (cw) excitation] the orthoexciton luminescence intensity as a function of temperature. They observed a striking minimum in the orthoexciton population near $T = 20$ K and an exponential increase above this temperature. The exponential increase above 20 K suggested that orthoexcitons and paraexcitons are in thermal equilibrium at the lattice temperature. The increase in orthoexciton population below 20 K suggested that slower interconversion at low temperature retains a larger non-equilibrium population in the higher-energy orthoexciton state.

Considering the electron and phonon symmetries at zone center, Caswell and Yu[5] proposed that ortho-para conversion proceeded by a two-phonon down-conversion process-one optical and one acoustic. Weiner *et al.*[6] made the first direct measurements of the interconversion rate by time-resolving the orthoexciton luminescence following subnanosecond laser excitation. The measured rate showed a roughly $T^{3/2}$ dependence plus a residual rate of about $(2.5\ \text{ns})^{-1}$ at low temperature, in contrast to the $T^{7/2}$ dependence predicted by the two-phonon model. The two-phonon mechanism became even less viable following time-resolved luminescence experiments by Snoke *et al.*,[9] who applied stress to the crystal to reduce the ortho-para splitting energy below that of the lowest energy optical phonon ($\Gamma_{25}^- = 10.7$ meV). No reduction in the ortho-para conversion rate was observed, eliminating the role of an optical phonon.

Snoke *et al.*[9] proposed that orthoexciton down-conversion is caused by emission of a single acoustic phonon. They developed a theory which predicted the temperature dependence of the down-conversion rate, but the rate went to zero at zero temperature, in contrast with experimental results.[6] Denev and Snoke[10] measured the orthoexciton lifetime as a function of applied stress, and developed a theory assuming the emission of a single longitudinal acoustic (LA) phonon. They use a deformation-potential Hamiltonian that does not take into account the spin-conversion process (see Sec. V). The form of the interaction Hamiltonian is a key issue in the present paper.

Finally, in an effort to understand the shorter lifetimes of orthoexcitons *at high densities*, Kavoulakis and Mysyrowicz[11] have proposed a two-body spin-flip mechanism for ortho-para conversion. The idea is that two orthoexcitons with opposite magnetic quantum numbers collide, exchange their electrons and holes via Coulomb interaction, and produce two paraexcitons. The model predicts an interconversion rate proportional to the density of orthoexcitons. However, a spin-flip scattering process conserves total exciton number, contrary to experimental evidence that both

orthoexcitons and paraexcitons are efficiently lost at high gas densities.[3,8,12,13] The experimental results favor an Auger recombination mechanism at high densities.

Our present experiments are conducted at low densities ($<10^{12}/\mathrm{cm}^3$), where the decay of orthoexcitons is observed to be independent of density. Excitons are observed by time-resolved photoluminescence. Orthoexcitons radiatively recombine either by a quadrupole-allowed transition or by phonon-assisted recombination, illustrated in Fig. 1(a). In contrast, direct paraexciton recombination is strictly forbidden, but phonon-assisted recombination is weakly allowed. As a result, the phonon-assisted luminescence from paraexcitons ($X_p-\Gamma_{25}^-$) is 500 times weaker than the phonon-assisted luminescence from orthoexcitons ($X_o-\Gamma_{12}^-$).

Due to these factors, measurement of the paraexciton population on a short time scale is difficult. High repetition rates are needed to optimize the paraexciton signal from a single pulse, and paraexcitons remaining from previous pulses must be accounted for properly. Also, during and (for a few nanoseconds) after a short excitation pulse the paraexciton luminescence is masked by scattered laser light and strong orthoexciton luminescence. Spectral filtering is required to isolate the paraexciton luminescence.

Using these techniques, we find that the buildup of the paraexciton population corresponds well to the decay of the orthoexciton population, verifying that we are dealing solely with the interconversion process.

This paper is organized as follows: In Sec. II the experimental setup for the measurement is described and the principal results are reported. In Sec. III we analyze the data with rate equations, considering in particular the effect of the background paraexciton buildup. In Sec. IV we propose that the ortho-para conversion is mediated by a TA-phonon process and compare the predictions of this theory to our measured interconversion rates as a function of temperature. In Sec. V we test the TA-phonon theory against new stress dependent data of the interconversion rate. Section VI gives our summary and conclusions.

II. EXPERIMENTAL METHODS AND RESULTS

Our experiments are performed on a natural-growth Cu_2O crystal cut with all (100) faces ($2\times2\times2.3$ mm^3). This crystal is one of those previously used to study the transport and thermodynamics of excitons.[12,14] We observe paraexciton lifetimes of 400–500 ns at 2–20 K, due to recombination at impurities. (Radiative recombination rates are known to be much longer.[13,15,16]) The crystal is mounted in an apparatus allowing the application of stress along [100], and the luminescence is collected along a [010] direction, perpendicular to the laser beam path.

A mode-locked and cavity-dumped dye laser produces a train of 5 ps pulses with a repetition time of 105 ns. The excitation wavelength of 600 nm corresponds to a 270 μm absorption length at $T=2$ K. To produce a low density gas of orthoexcitons ($<10^{12}/\mathrm{cm}^3$) and avoid the complications of diffusion,[12] we defocus the laser beam and use an average incident power less than 5 mW. The luminescence is spectrally dispersed by a half-meter spectrometer with 16 Å/mm

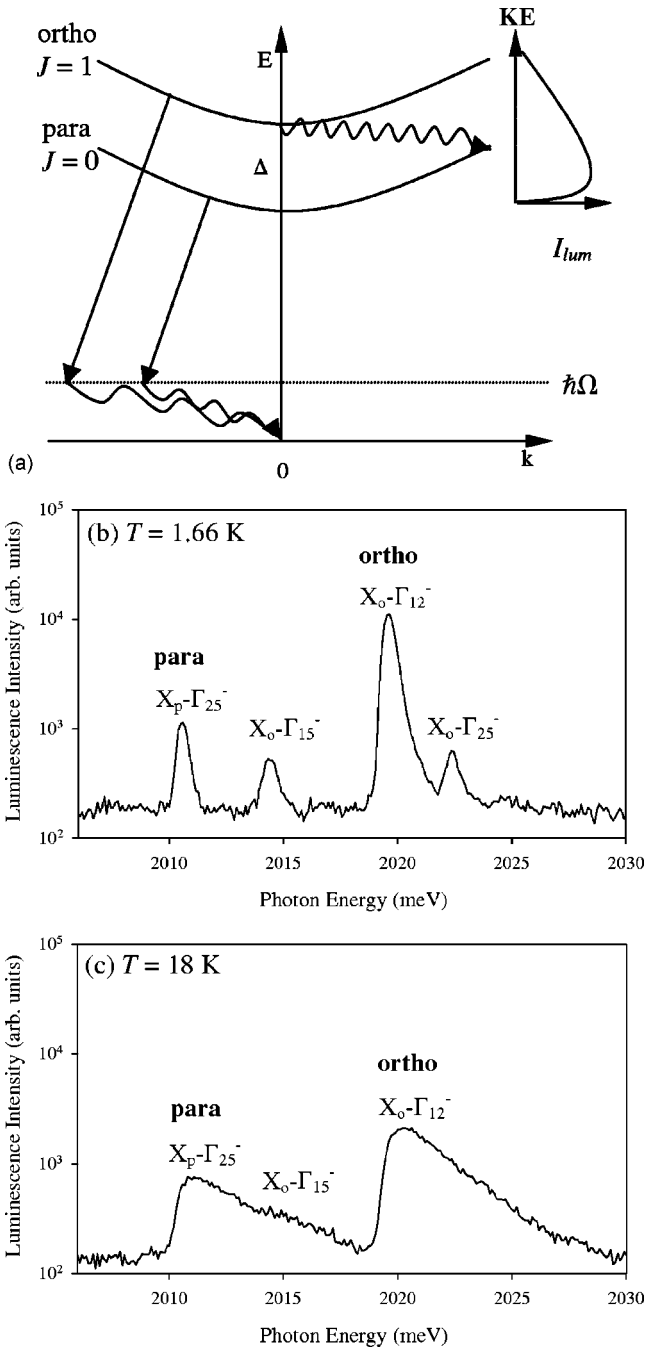

FIG. 1. (a) Schematic diagram of the exciton relaxation kinetics at low densities. Wavy arrows denote phonon emission; straight arrows photon emission. $\hbar\Omega$ is the optical phonon energy. The time-integrated photoluminescence is given for (b) $T=1.66$ K and (c) $T=18$ K. For $T>15$ K, the $X_p-\Gamma_{25}^-$ line starts to overlap with the $X_o-\Gamma_{15}^-$.

dispersion, and detected by a Hammamatsu multichannel-plate photomultiplier tube using time-correlated single-photon counting. We measure an overall time response of 70 ps.

Figures 1(b) and 1(c) show time-integrated luminescence spectra at 1.66 and 18 K. At temperatures greater than about 15 K, the paraexciton line ($X_p-\Gamma_{25}^-$) starts to overlap with the orthoexciton line ($X_o-\Gamma_{15}^-$), so care must be taken to

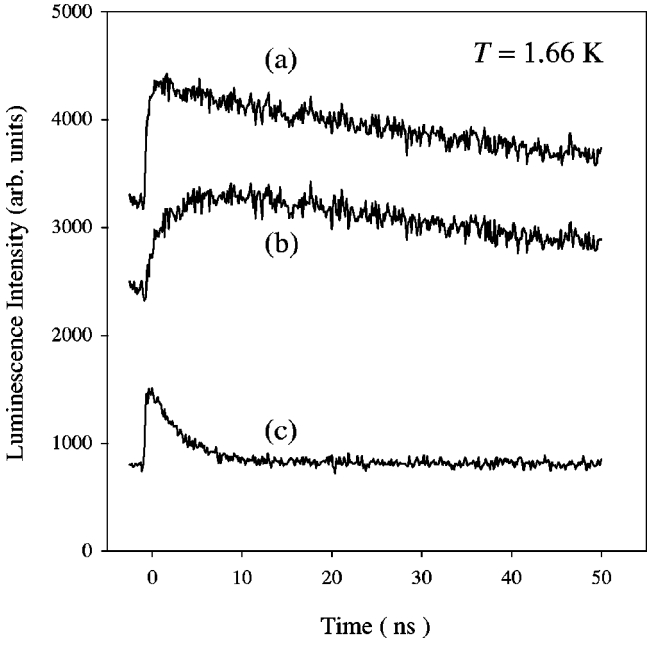

FIG. 2. Trace (a) is the buildup of spectrally integrated $X_p - \Gamma_{25}^-$ paraexciton spectrum following a 5 ps laser pulse. This raw data includes a base line from previously produced paraexcitons plus a background due to scattered light from the laser and strong orthoexciton luminescence. Trace (c), obtained at an energy just below the paraexcitons spectrum, shows the transient scattered light. Trace (b) equals trace (a) minus trace (c) and corresponds to the buildup of paraexcitons at $T = 1.66$ K plus the residual decaying signal from paraexcitons created in previous pulses.

isolate the signals from the two species. For these cw spectra, the paraexciton luminescence is comparable to the orthoexciton luminescence because we are taking advantage of the much longer paraexciton lifetime.

On a nanosecond time scale the paraexciton signal is 500 times weaker than that of the orthoexcitons. We eliminate scattered laser light and background luminescence from orthoexciton replicas by using a 620 nm interference filter angle-tuned to the maximum phonon-assisted paraexciton signal at 615 nm. The interference filter reduces the paraexciton signal by about a factor of 4 while reducing the background by a factor of a thousand.

Figure 2 indicates the care that must be taken to obtain the paraexciton buildup in the presence of scattered light from the laser and strong orthoexciton luminescence. Trace (a) shows the buildup of luminescence collected from the integrated paraexciton spectrum. The actual paraexciton buildup, trace (b), is obtained by subtracting off the background luminescence shown in trace (c). As one can see, this procedure is absolutely necessary to obtain the correct time dependence of the paraexciton buildup. Notice that in trace (b) there is a residual signal at $t < 0$ that we attribute to paraexctions created in earlier pulses (repetition time = 105 ns). The residual signal must be accounted for in order to determine the impurity-induced exciton recombination time (about 450 ns), insuring that we have properly accounted for this effect as a function of temperature.

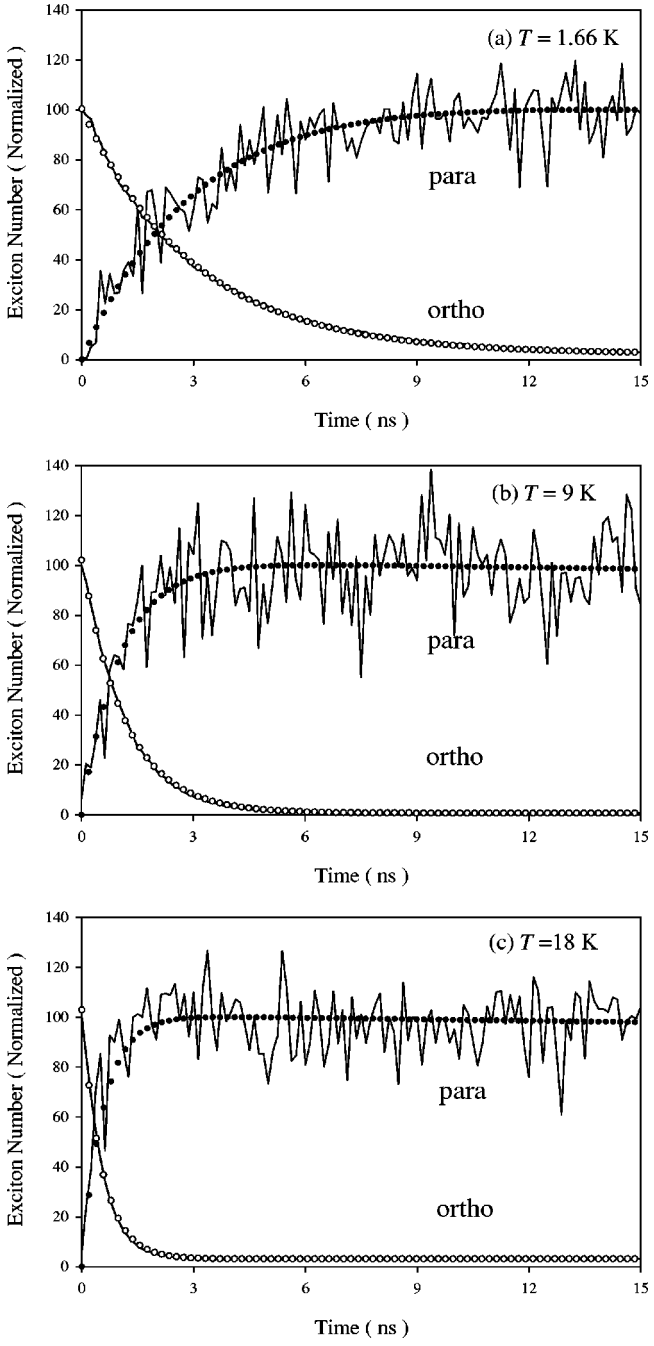

FIG. 3. Normalized temporal behaviors of excitons after subtracting the residual paraexciton signal. Circles and dots are fits of Eqs. (3) and (4) to the data. The conservation of total exciton number is confirmed by adding the two curves at each temperature (not shown). The sum decays via the nonradiative recombination process.

Also shown in Fig. 3 is the time trace from orthoexcitons, normalized by their radiative efficiency compared to the paraexcitons. The relative luminescence rates are well known from the corresponding absorption strengths.[17] Data collection times for orthoexcitons and paraexcitons are 20 and 1800 s, respectively.

III. DIRECT MEASUREMENT OF THE DOWN-CONVERSION RATE

For an excitation wavelength of 600 nm ($h\nu = 2065.8$ meV), the paraexciton generation is negligible, known from assignment of the absorption bands near 600 nm. Orthoexcitons are created by the Γ_{12}^{-} phonon-assisted absorption process. The rate equations governing the populations of the orthoexciton (o) and paraexciton (p) levels are

$$\frac{dN_o}{dt} = -DN_o + UN_p - \gamma_o N_o + G(t), \tag{1}$$

$$\frac{dN_p}{dt} = -UN_p + DN_o - \gamma_p N_p, \tag{2}$$

where N, γ, and G are the number of excitons, the recombination rates, and the generation rate. U and D are the up- and down-conversion rates. For 5 ps excitation pulses, $G(t)$ can be approximated by a delta function. Also $U/D \ll 1$ and the γ's are much smaller than D at the temperatures considered ($T < 20$ K). In this paper we refer to D as either the "down-conversion" or "interconversion" rate. Under these conditions the solutions to the simultaneous rate equations are given by

$$N_o(t) = N_o(0)e^{-(D+\gamma_o)t}, \tag{3}$$

$$N_p(t) = N_o(0)[e^{-\gamma_p t} - e^{-(D+\gamma_o)t}]. \tag{4}$$

Because the radiative recombination times are different for the two species ($\tau_p/\tau_o = 500$ for the two phonon replicas), the intensity ratio between orthoexcitons and paraexcitons is given by

$$\frac{I_o}{I_p} = \frac{N_o/\tau_o}{N_p/\tau_p} = 500\frac{N_o}{N_p}. \tag{5}$$

In Fig. 3 we plot the temporal behavior of paraexciton luminescence at three different temperatures, with the residual signal from prepulse paraexcitons subtracted. Superimposed is the orthoexciton signal normalized as described earlier to reflect the relative number of excitons. The fit to the tail of the paraexciton luminescence yields a paraexciton recombination rate γ_p of about $(450\ \text{ns})^{-1}$. At these relatively low excitation levels, this decay rate does not change with laser power (i.e., exciton density); therefore, we conclude that the paraexciton decay is due to nonradiative recombination at impurities. The impurity-induced decay rate for orthoexcitons γ_o is not obtainable from our data due to the rapid down-conversion rate. In the analysis later, we assume that the impurity recombination rates are the same for ortho and paraexcitons ($\gamma \equiv \gamma_o = \gamma_p$), an assumption that has little effect in the determination of the down-conversion rate D.

A fit of the orthoexciton decay curve to Eq. (3) (circles) yields the decay rate $D+\gamma_o$. An independent measurement of $D+\gamma_o$ is obtained from a fit of the paraexciton transient to Eq. (4) (dots). The agreement between the final density (at 15 ns) of the paraexcitons with initial density of orthoexcitons confirms that the orthoexciton decay is entirely due to down-conversion into paraexcitons. That is, there is no loss of excitons during the interconversion process except for slow nonradiative recombinations at impurities confirmed by the sum of Eqs. (3) and (4), $N_o + N_p \propto e^{-\gamma t}$, with $\gamma = (450\ \text{ns})^{-1}$.

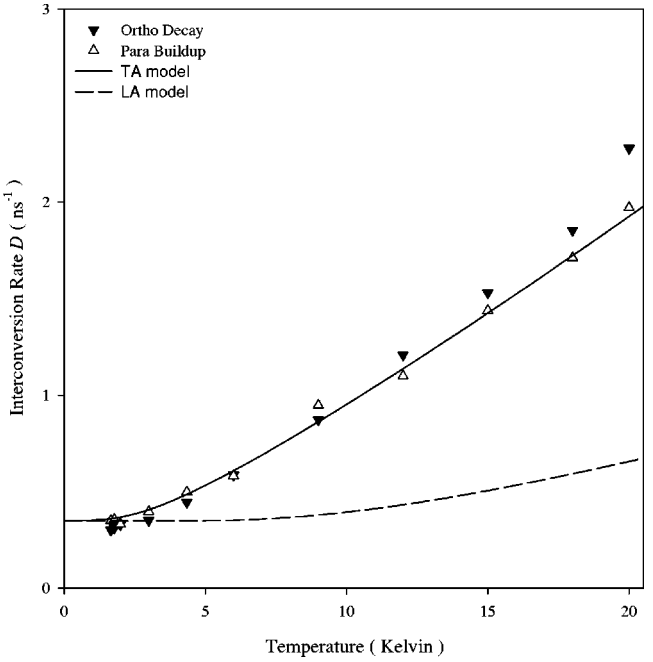

FIG. 4. Temperature dependence of the down-conversion rates, $D = (D+\gamma_o) - \gamma_p$, determined from the orthoexciton decay rates ($D + \gamma_o$, solid triangles) and paraexciton buildup rates ($D+\gamma_o$, open triangles), assuming $\gamma_o = \gamma_p$ and a value of γ_p that is determined from the paraexciton decay. Our data are within the error bars of orthoexciton decay rates reported by Weiner *et al.*[6] The solid line corresponds to the TA-phonon process discussed in the text, scaled by a single fitting parameter. The temperature dependence, approximately given by Eq. (6), depends strongly on the phonon velocity involved. The dashed line is the LA-phonon process,[10] involving 3.5 times larger phonon velocity.

In Fig. 4 we plot the interconversion rate D from both orthoexciton decay rates and paraexciton buildup rates for temperatures ranging from 2 to 20 K. The orthoexciton decay rates agree quite well with the paraexciton buildup rates. Small differences at the higher temperatures may be due to inaccuracies in obtaining the integrated paraexciton signal as it begins to overlap the orthoexciton replica. The solid and dashed curves shown in Fig. 4 are theoretical fits described in the next section.

IV. OTHO-PARA CONVERSION BY TA PHONONS

If the ortho-para conversion involves scattering of acoustic phonons, then the rate should increase with temperature. Specifically, phonon *emission* will contribute a rate proportional to $1+n$ where n is the occupation number of the relevant phonons, and phonon *absorption* will contribute a rate proportional to n. As indicated in Fig. 1(a), the phonon energy is relatively small compared to the energy difference Δ between ortho- and paraexcitons, so the transition is nearly

horizontal. The phonon momentum is thus nearly $\sqrt{2m\Delta}$ and the phonon energy is $v\sqrt{2m\Delta}$, where v is the transverse or longitudinal sound velocity, depending on which phonon branch is involved.

At high temperatures ($T \gg v\sqrt{2m\Delta}/k_B \sim 5$ K for TA and ~ 20 K for LA) the phonon occupation number is approximately $n=(k_BT)/(v\sqrt{2m\Delta})$. Considering both phonon emission and absorption, the temperature dependence of the down-conversion rate is roughly proportional to $1+2n$, yielding

$$D(T) \propto 1 + \frac{2k_BT}{v\sqrt{2m\Delta}}. \tag{6}$$

From Eq. (6) we see that the temperature dependence is determined by the phonon velocity. In Cu_2O, the velocities of the longitudinal and transverse phonons differ by a factor of about 3.5 ($v_L=4.5$ km/s, $v_T=1.3$ km/s). LA phonon emission produces the temperature dependence shown in the dashed curve of Fig. 4, while the TA-phonon-mediated process predicts the solid curve. (These curves take into account the actual distribution of exciton energies and phonon occupation numbers, as discussed later in this section.) The data clearly indicate that the lower-velocity TA phonons are involved. Notice that the only fitting parameter is the overall scaling factor. Our conclusion relies on a good measurement of the low-T limit of D and a proof that the limiting orthoexciton decay was not caused by some other mechanism than down-conversion. The rate as $T \to 0$ is 0.30 ± 0.04 ns^{-1}.

How do the phonon polarization and symmetry enter into the physics? Caswell and Yu[6] pointed out that conversion of an orthoexciton (Γ_{25}^+) to a paraexciton (Γ_2^+) should involve a Hamiltonian with symmetry $\Gamma_{25}^+ \otimes \Gamma_2^+ = \Gamma_{15}^+$. We disagree with Refs. 6 and 10 regarding their treatment of the lattice phonon scattering as an odd-parity, Γ_{15}^-, interaction. Acoustic phonons precisely at zone center do transform as a displacement, Γ_{15}^-, but the uniform lattice displacement of these infinite-wavelength phonons should not be expected to affect the exciton spin state. Finite-wave-vector phonons cause compression (Γ_1^+), shear (Γ_{12}^+ and Γ_{25}^+), and rotation (Γ_{15}^+) in amounts proportional to the phonon wave vector. Here we examine the possibility that the rotation (Γ_{15}^+) associated with TA phonons drives the spin-exchange process (ortho-para interconversion).

Lattice rotation will rotate the atomic orbitals from which the conduction and valence bands are built, and rotation of these orbitals will affect the electron and hole spin through spin-orbit coupling. To predict the down-conversion rate we solve the somewhat simplified 12-state system including the electron and hole spins, with angular momentum operators $\mathbf{S}^e$ and $\mathbf{S}^h$, and the three degenerate (before spin-orbit coupling) valence band orbitals, with pseudo-angular momentum operator $\mathbf{L}$. This system has been treated by Waters *et al.*[18] and a more complete model has been developed by Trebin *et al.*[19] The static Hamiltonian, allowing for strains ϵ_{ij} in the crystal, is

$$H = \frac{2\alpha}{3}\mathbf{L}\cdot\mathbf{S}^h + 2J\mathbf{S}^e\cdot\mathbf{S}^h + b\sum_{i=x,y,z}\epsilon_{ii}(3L_i^2 - L^2), \tag{7}$$

where $\alpha=132$ meV is the spin-orbit splitting, $J=-23$ meV is the exchange interaction, and $b=-1.2$ eV is the anisotropic deformation potential for the holes. These parameters are determined by fitting the spectroscopically measured energies of the 1s ortho- and paraexcitons.

When TA phonons rotate the lattice through the angle $\frac{1}{2}\nabla\times\mathbf{u}$, where $\mathbf{u}$ is the lattice displacement field, we assume the spatial wave functions follow the lattice, while the spin parts of the wave functions move according to the spin-orbit and exchange Hamiltonian in Eq. (7). Working in a nonrotating frame of reference, rotation perturbs the Hamiltonian by changing $\mathbf{L} \to \mathbf{L} + \frac{1}{2}(\nabla\times\mathbf{u})\times\mathbf{L}$. We treat the additive term in the spin-orbit Hamiltonian as a perturbation

$$H' = \frac{\alpha}{3}[(\nabla\times\mathbf{u})\times\mathbf{L}]\cdot\mathbf{S}^h = \frac{\alpha}{3}(\mathbf{L}\times\mathbf{S}^h)\cdot(\nabla\times\mathbf{u}). \tag{8}$$

We must evaluate the matrix element of H' between the yellow orthoexciton and yellow paraexciton eigenstates of Eq. (7). Waters *et al.*[18] list eigenstates ϕ_1 through ϕ_{12} which diagonalize the spin-orbit part of Eq. (7). We use these states as a basis in which to solve the full Hamiltonian. To first order in J/α and in $b\epsilon_{zz}/\alpha$, the yellow paraexciton is

$$|\text{para}\rangle = \phi_{12} - \frac{\sqrt{2}b\epsilon_{zz}}{\alpha}\phi_{11},$$

and the yellow orthoexcitons are

$$|\text{ortho}_z\rangle = \phi_{10} - \frac{2\sqrt{2}J}{3\alpha}\phi_9 - \frac{\sqrt{2}b\epsilon_{zz}}{\alpha}\phi_9,$$

$$|\text{ortho}_x\rangle = \phi_5 - \frac{2\sqrt{2}J}{3\alpha}\phi_4 + \frac{b\epsilon_{zz}}{\sqrt{2}\alpha}\phi_4 - \frac{\sqrt{3}b\epsilon_{zz}}{\sqrt{2}\alpha}\phi_3,$$

$$|\text{ortho}_y\rangle = \phi_8 - \frac{2\sqrt{2}J}{3\alpha}\phi_7 + \frac{b\epsilon_{zz}}{\sqrt{2}\alpha}\phi_7 + \frac{\sqrt{3}b\epsilon_{zz}}{\sqrt{2}\alpha}\phi_6. \tag{9}$$

When the perturbation H' acts on the paraexciton, the result involves

$$(\mathbf{L}_x\mathbf{S}_y^h - \mathbf{L}_y\mathbf{S}_x^h)|\text{para}\rangle = -\frac{\phi_9}{\sqrt{2}} - \frac{b\epsilon_{zz}}{\alpha}\phi_{10}, \tag{10}$$

where we have considered only the z component of the curl. Thus the rotation of the lattice by a TA phonon connects the ortho- and paraexciton with a matrix element

$$M_{\text{op}} = \langle\text{ortho}_z|H'|\text{para}\rangle = \frac{2J}{9}(\nabla\times\mathbf{u})\cdot\hat{\mathbf{z}}. \tag{11}$$

The other components of $\nabla\times\mathbf{u}$ connect the paraexciton to each of the other two orthoexcitons.

We were surprised to find in Eq. (10) that there is no term in ϕ_{10} to zeroth order in J, so that to this order the matrix element in Eq. (11) is zero. That is, $\langle\phi_{10}|H'|\phi_{12}\rangle=0$. Also note that the terms proportional to $b\epsilon_{zz}$ exactly cancel in Eq. (11).

We quantize the lattice vibrations $\mathbf{u}$ and apply Fermi's golden rule to calculate the transition rate induced by M_{op}. Under conditions of zero temperature, zero orthoexciton momentum and only spontaneous emission of a phonon, the rate is

$$\Gamma_{\mathrm{op}}^{z} = \frac{2\pi}{\hbar}\int \frac{d^3\mathbf{q}}{(2\pi)^3}\left|\frac{2J\sin\theta}{9}\right|^2 \frac{q\hbar}{2\rho v}\delta\left(\Delta - \hbar v q - \frac{\hbar^2 q^2}{2m}\right)$$
$$= \left(\frac{2J}{9}\right)^2 \frac{q_\Delta^3/3\pi\rho v}{\hbar v + \hbar^2 q_\Delta/m}, \tag{12}$$

where the sine of the angle θ between the phonon wave vector $\mathbf{q}$ and $\hat{\mathbf{z}}$ picks out the z-component of $\nabla\times\mathbf{u}$, and where $\hbar q_\Delta = \sqrt{2m\Delta + m^2v^2} - mv$ denotes the phonon momentum as determined by energy conservation and $\rho = 6.1\ \mathrm{g/cm^3}$ is the mass density of Cu_2O. Equation (12) is a prediction for the absolute down-conversion rate for the state $|\mathrm{ortho}_z\rangle$ at zero temperature. With an exchange splitting $J = -23$ meV derived from the spectroscopic ortho-para splitting, it predicts a rate of $0.002\ \mathrm{ns}^{-1}$, which is 150 times smaller than the observed rate, $0.3\ \mathrm{ns}^{-1}$.

There are several factors that increase the theoretical rate estimated earlier. First, the green exciton binding energy is greater than that of the yellow exciton, making the energy splitting between the 1*s* excitons only 58% of the full spin-orbit interaction α. The energy denominators in Eq. (9) should have this reduced energy $\alpha' = 0.58\alpha$ instead of α, while the interaction in Eq. (8) still has the full spin-orbit interaction. This correction multiplies Eq. (12) by $(\alpha/\alpha')^2 = 3.0$.

Second, the different binding energies imply a greater electron-hole overlap in the more tightly bound green excitons. We should thus expect a larger exchange coupling for the green excitons. Waters estimated $J_y \approx 0.5J$ and $J_g \approx 2.0J$ where J now represents the geometric mean of two constants. Then $J_y = -23$ meV to match the observed yellow ortho-para splitting, and the geometric mean $J = -46$ meV appears in Eq. (9) and thus in the matrix element.

With these two factors taken into account the predicted rate is $0.024\ \mathrm{ns}^{-1}$ or about 1/12 the observed rate. Most seriously, our restriction to 1*s* states ignores the strong mixing that exists between the green 1*s* orthoexciton (the state ϕ_9) and yellow 2*s* orthoexciton.[19] A more accurate wave function ϕ_9, for use in Eqs. (8) and (9), would require solution of the radial wave function of the excitons.

We believe that the preceding theory captures the essence of the dominant down-conversion process for excitons in Cu_2O, based on its agreement with the temperature and (see later) the stress dependence of the rate, and because it comes close to predicting the order of magnitude of the rate (within a factor of 3.5 in matrix element). This model, extended to finite temperature and numerically integrated over the thermal distribution of orthoexcitons, is the solid curve in Fig. 4. The predicted rate has been scaled up to compare its temperature dependence with the experimental data, yielding excellent agreement. The TA phonon velocity ($v_T = 1.3$ km/s) sets the temperature of the turnover to the observed dependence at higher T. For comparison in Fig. 4, we show the T-dependence assuming the LA phonon velocity, which yields a poor fit to the data.

V. STRESS DEPENDENCE OF THE DOWN-CONVERSION RATE

Strain changes the exciton states significantly. Extending the perturbative treatment of the previous section, stress dependence of the down-conversion rate first appears in higher-order terms proportional to both exchange coupling and strain. The orthoexciton state that is *raised* in energy under compressive strain ($b\epsilon_{zz} > 0$) has an increased down-conversion rate

$$\langle \mathrm{ortho}_z|H'|\mathrm{para}\rangle = \left(\frac{2J}{9} + \frac{2Jb\epsilon_{zz}}{3\alpha}\right)(\nabla\times\mathbf{u})\cdot\hat{\mathbf{z}}. \tag{13}$$

The two orthoexciton states that are *reduced* in energy have their down-conversion rate reduced

$$\langle \mathrm{ortho}_x|H'|\mathrm{para}\rangle = \left(\frac{2J}{9} - \frac{Jb\epsilon_{zz}}{3\alpha}\right)(\nabla\times\mathbf{u})\cdot\hat{\mathbf{z}}, \tag{14}$$

and it is these orthoexcitons that are observed in the strain well experiments reported both here and in Ref. 10.

Denev and Snoke[10] have reported a study of exciton relaxation as a function of stress in a Hertzian strain well. Their principal aim was characterization of the Auger recombination rate at high exciton densities; however, as mentioned earlier they also measured orthoexciton lifetimes versus stress at lower densities. Their analysis involved several adjustable parameters and required a correction for a rather short (20 ns) paraexciton lifetime in their sample. On the theoretical side, their deformation-potential Hamiltonian has even parity and cannot connect the even parity orthoexciton state and the odd parity intermediate state introduced by $\mathbf{k}\cdot\mathbf{p}$ perturbation.

We have conducted similar low-density measurements on our sample,[20] which has about 20 times weaker impurity recombination than Ref. 10. We have made measurements from zero to 6 kbar, corresponding to changing Δ from 12 to 3.4 meV.

Figure 5 shows the decay of orthoexcitons in the strain well for increasing values of stress at a temperature of 2 K. The experimental lifetimes are plotted as a function of exchange splitting Δ in Fig. 6. The lifetimes increase by an order of magnitude, from 3 ns at zero stress to 30 ns at 6 kbar. The solid curve is the orthoexciton lifetime from the low-temperature down-conversion rate, calculated by numerical diagonalization of the Hamiltonian Eq. (7). For comparison, the dashed line in Fig. 6 shows the prediction if, instead, the LA-phonon velocity is used in the calculation. Again, the data clearly prefers the TA-phonon velocity, which is required in the theory.

An approximate analytic expression for the down-conversion rate is obtained by using Eq. (14), giving the explicit Δ (in meV) dependence of the rate at 0 K:

$$D(\Delta) = \left(\frac{2J}{9} + \frac{3(12-\Delta)}{8}\right)^2 \frac{2m^2\Delta}{3\pi\rho v_T\hbar^4}. \tag{15}$$

To this order, at finite temperature, $D(\Delta, T)$ is given by this expression multiplied by $1+2n$ as discussed in the previous section.

VI. SUMMARY AND CONCLUSIONS

Experiments and theory have been zeroing in on the interconversion mechanism since the first time-resolved ex-

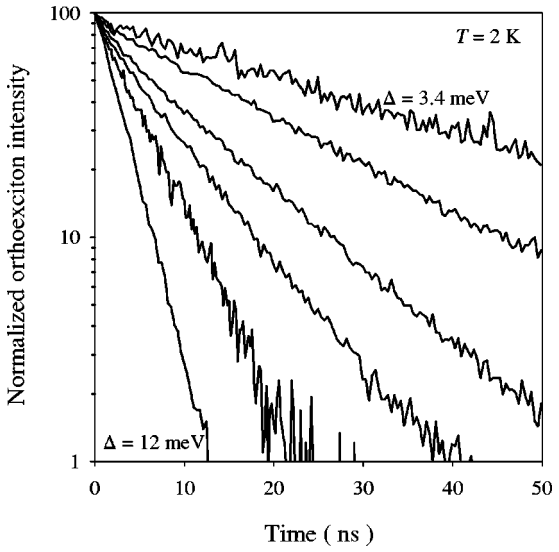

FIG. 5. Normalized orthoexciton decay curves at $T=2$ K for $\Delta=3.4$, 4.5, 5.7, 6.9, 9.3, and 12 meV. The exchange splitting Δ is determined from the orthoexciton shift with stress, as detailed in Ref. 21. Our measured values of orthoexciton lifetime are approximately 30% larger than those reported by Denev and Snoke.[10] Their measurement may have been affected by the significantly shorter non-radiative decay of excitons in their sample.

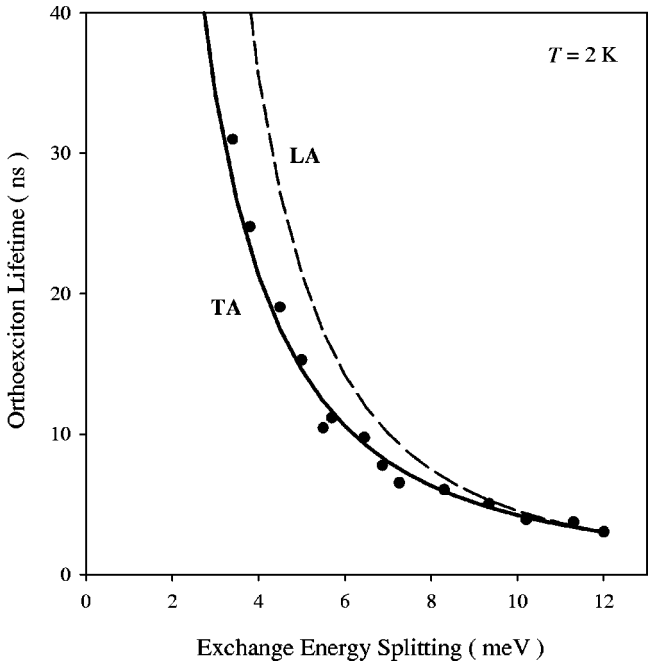

FIG. 6. Stress dependence of the orthoexciton lifetime at $T=2$ K. The dots are measured lifetimes as a function of the energy splitting. The solid line corresponds to the TA-phonon process with the same scaling parameter determined as in the temperature dependence of Fig. 4. The dashed line corresponds to the LA-phonon process.

periments by Caswell and Yu. Our experiments are the first to observe both orthoexciton and paraexciton populations during equilibration. A pulsed laser resonantly creates orthoexcitons, which decay into paraexcitons with the down-conversion rate D. The rate of conversion between yellow orthoexcitons and yellow paraexcitons in cuprite has been isolated and measured as a function of temperature and as a function of energy splitting between the states.

In our natural growth, high purity samples we find that the exciton number is conserved during the thermalization process, leading to an accurate determination of the interconversion rate D over a wide range of temperatures and sample stress, which is used to vary the exchange splitting Δ.

Both the temperature and stress dependence of D that we measure are well explained by a model of orthoexciton down-conversion by emission of a single TA phonon. The essential results are contained in Figs. 4 and 6, which compare our data to the TA-phonon model with only a single overall scaling factor. The emission of a single TA phonon is a physically reasonable model, which not only fits both functional dependencies but also yields the absolute magnitude of the matrix element within a factor of 3.5. The remaining discrepancy may be due to an imperfect knowledge of mixing between green and yellow exciton states. We emphasize that no other theory to date has attempted to predict the *absolute* spin-conversion rate for excitons.

ACKNOWLEDGMENTS

This material is based upon work supported by the U.S. Department of Energy, Division of Materials Sciences under Award No. DEFG02-91ER45439, through the Frederick Seitz Materials Research Laboratory at the University of Illinois at Urbana-Champaign. Experiments were conducted in the MRL Laser and Spectroscopy Facility.

[1] J. B. Grun, M. Seiskind, and S. Nikitine, J. Phys. Chem. Solids **19**, 189 (1961). The value quoted here is actually the zero-T value.

[2] S. A. Moskalenko and D. W. Snoke, *Bose-Einstein Condensation of Excitons and Biexcitons* (Cambridge University Press, Cambridge, 2000). Appendix A deals particularly with Cu_2O.

[3] For a recent analysis, see, K. E. O'Hara and J. P. Wolfe, Phys. Rev. B **62**, 12 909 (2000).

[4] F. I. Kreingold and V. L. Marakov, Fiz. Tverd. Tela (Leningrad) **15**, 1307 (1973) [Sov. Phys. Solid State **15**, 890 (1973)].

[5] N. Caswell and P. Y. Yu, Phys. Rev. B **25**, 5519 (1982).

[6] J. S. Weiner, N. Caswell, P. Yu, and A. Mysyrowicz, Solid State Commun. **46**, 105 (1983).

[7] K. E. O'Hara, J. R. Guillingsrud, and J. P. Wolfe, Phys. Rev. B **60**, 10 872 (1999).

[8] J. T. Warren, K. E. O'Hara, and J. P. Wolfe, Phys. Rev. B **61**, 8215 (2000).

[9] D. Snoke, D. P. Trauernicht, and J. P. Wolfe, Phys. Rev. B **41**, 5266 (1990).

[10] S. Denev and D. W. Snoke, Phys. Rev. B **65**, 085211 (2002). The

theoretical curve in their Fig. 2 assumes an LA-phonon velocity [D. W. Snoke (private communication)].

[11] G. M. Kavoulakis and A. Mysyrowicz, Phys. Rev. B **61**, 16 619 (2000).

[12] D. P. Trauernicht and J. P. Wolfe, Phys. Rev. B **33**, 8506 (1986).

[13] K. E. O'Hara, L. Ó Súilleabháin, and J. P. Wolfe, Phys. Rev. B **60**, 10 565 (1999).

[14] D. P. Trauernicht, A. Mysyrowicz, and J. P. Wolfe, Phys. Rev. B **28**, 3590 (1983).

[15] A. Mysyrowicz, D. Hulin, and A. Antonetti, Phys. Rev. Lett. **43**, 1123 (1979).

[16] See, for example, the review by J. P. Wolfe, J. L. Lin, and D. W. Snoke, in *Bose-Einstein Condensation*, edited by A. Griffin, D. W. Snoke, and S. Stringari (Cambridge University Press, Cambridge, 1995), p. 281.

[17] P. D. Bloch, and C. Schwab, Phys. Rev. Lett. **41**, 514 (1978).

[18] R. G. Waters, F. H. Pollack, R. H. Bruce, and H. Z. Cummins, Phys. Rev. B **21**, 1665 (1980).

[19] H.-R. Trebin, H. Z. Cummins, and J. L. Birman, Phys. Rev. B **23**, 597 (1981).

[20] In these experiments we use a stressor with 5 mm radius of curvature and excite the Γ_{12}^{-}-phonon-assisted orthoexciton band, tuning the laser to about 1 meV above the band edge as the applied stress is changed. In this way, excitons are created only in the well, which is necessary to avoid complicating migration effects. The laser beam is defocused to the size of the well to avoid diffusion effects, and the luminescence is collected over the central 30% of the well. With these methods, consistent results were obtained.

[21] K. E. O'Hara, Ph.D. thesis, University of Illinois, 1999.